Journal of Sound and Vibration 441 (2019) 50–62

Contents lists available at ScienceDirect

Journal of Sound and Vibration

journal homepage: www.elsevier.com/locate/jsvi

Acoustic loading beneath hypersonic transitional and turbulent boundary layers

K. Ritos [a, *], D. Drikakis [b, **], I.W. Kokkinakis [a]

[a] Department of Mechanical and Aerospace Engineering, University of Strathclyde, Glasgow, UK
[b] University of Nicosia, Nicosia, Cyprus

ARTICLE INFO

Article history:
Received 27 March 2018
Received in revised form 1 October 2018
Accepted 13 October 2018
Available online 22 October 2018
Handling Editor: Paolo Tiso

Keywords:
Acoustic loading
Transition
Turbulence
Multimode
Compressible flows
Implicit Large Eddy Simulations

ABSTRACT

This paper concerns a study of pressure fluctuations beneath hypersonic transitional and turbulent boundary layers and associated acoustic loading on a flat surface. We have employed high-order implicit large eddy simulations in conjunction with the atmospheric (von Kármán) multimode energy spectrum as initial condition, and conducted simulations at Mach 4, 6 and 8 and for different inflow turbulence intensities. The spectral analysis of the pressure fluctuations shows consistent results with the available theoretical, experimental and numerical data for fully turbulent boundary layers. In the transition region the spectrum roll-off diverges from the existing scaling predictions for incompressible, as well as fully-turbulent compressible flows. This study shows that the spectrum in the transition region is governed by different scaling laws. The Mach number has a direct impact on the spectrum for both transitional and fully turbulent flows, especially in the high-frequency region of the spectrum. Increasing the inlet turbulence intensity leads to higher amplitude pressure fluctuations in the mid-to-high-frequency region, faster transition to turbulence, and higher acoustic loading on the solid surface.

1. Introduction

Pressure fluctuations within supersonic and hypersonic transitional and turbulent boundary layers (TBLs) are a dominant cause of acoustic fatigue that structural elements of an aircraft are exposed to, according to Bull [1]. It has been shown that the pressure fluctuations and heating rates in boundary-layer transition are higher than the observed in a fully turbulent boundary layer [2]. The periodic intermittent spatial-temporal alternation between laminar and turbulent regions produce a broad spectrum of disturbances that leads to these high pressure fluctuations.

Supersonic TBLs have been extensively studied focusing on the amplitude of pressure fluctuations [3] and the roll-off of the pressure spectrum [4–6]. Based on incompressible data and conventional (noisy flow) hypersonic wind-tunnel measurements an attempt to establish a correlation between transitional and turbulent pressure fluctuations was made [7]. These initial attempts did not accurately predict the transitional pressure fluctuations.

The linear stability theory [8] shows that multiple instability modes exist in high-speed boundary layers, contrary to low-speed or incompressible boundary layers where only one mode exist (Tollmien-Schlichting). Moreover, the transition process

* Corresponding author.
** Corresponding author.
E-mail addresses: konstantinos.ritos@strath.ac.uk (K. Ritos), drikakis.d@unic.ac.cy (D. Drikakis).

https://doi.org/10.1016/j.jsv.2018.10.021

in hypersonic boundary layers is highly random due to the existence of higher modes. The random nature of the hypersonic transition process explains its sensitivity to changes in the disturbance environment that can significantly change the transition process [9]. Contrary to previous studies that focused on single mode or 'controlled' transition, this paper focuses on multi-mode perturbations, which comprise a large number of waves imitating the von Kármán atmospheric turbulence.

Although hypersonic TBLs and transitional flows have been studied experimentally during the recent years [10–13], numerical studies are limited [9,14,15]. Furthermore, high-resolution investigations of TBLs on acoustic loading are indeed scarce [16]. To the best of the authors' knowledge studies for the frequency content of pressure fluctuations in attached transitional boundary layers at supersonic and hypersonic speeds have not been carried out. Experiments in transitional hypersonic boundary layers, not necessarily over a flat plate, have been performed in the past with a characteristic example being the work of Casper et al. [13] and references therein.

The aim of this work is to present spatial and spectral analysis of pressure fluctuations beneath a transitional hypersonic boundary layer in conjunction with a von Kármán atmospheric-like inflow condition. Simulations have been performed at Mach 4, 6 and 8 and turbulence intensities in the range of 0.5%–3% of the free stream velocity. The results are compared with available Direct Numerical Simulations (DNS) and experimental data in the fully turbulent region, and the accuracy of theoretical predictions is also investigated.

2. Computational model

The problem considered in this study concerns hypersonic flow over a flat plate subjected to von Kármán atmospheric spectrum at the inlet. The flow transitions to fully turbulent downstream of the plate. The implicit Large Eddy Simulation (iLES) approach has been employed in the framework of the high-order code CNS3D, which has been used in the past across a range of iLES studies for transitional and turbulent flows [17–19]. CNS3D is based on the HLLC Riemann solver [20] and a ninth-order WENO scheme [21] for the advective terms, second-order discretisation for the viscous terms and the third-order accurate Runge-Kutta method for the time integration [22].

It has been shown that shock-capturing, finite volume, Godunon-type methods are suited for the simulation of compressible turbulent flows in the numerical framework of iLES [22,23]. Furthermore, the order of spatial discretisation in iLES significantly influences the turbulence scales captured [24,25]. High-order iLES for wall-resolved subsonic, supersonic and hypersonic turbulent boundary layers can be found in Refs. [18,19,24,26,27].

Simulations were performed at Mach 4, 6 and 8 and for turbulence intensities, $Tu = 0.5$, 1 and 3% of the free-stream velocity. The free-stream flow conditions correspond to earth standard atmosphere at an altitude of $h = 12$ km, where the free-stream density, pressure, and temperature are $\rho_\infty = 0.3124\,\mathrm{kg/m^3}$, $P_\infty = 19.417$ kPa and $T_\infty = 216.64$ K, respectively. The incoming flow has a Reynolds number, Re, of 52, 000, 78, 000 and 104, 000 for the $M = 4$, 6 and 8 cases, respectively; the Re number calculation is based on the free-stream properties and the distance ($x_l = 2$ mm) required for a Blasius profile of a given thickness to be developed.

The simulation domain is a rectangular cuboid that starts at the position x_l and has dimensions $100 \times 6 \times 6$ mm. Periodic boundary conditions are implemented in the spanwise direction (z). On the wall, no-slip isothermal conditions are employed with a temperature T_w of 820 K, 1600 K and 2700 K, for $M = 4$, 6 and 8, respectively. These temperatures have been chosen to be close to the adiabatic recovery temperature for each Mach number, thus excluding wall cooling or heating effects. Supersonic outflow conditions are imposed at the outlet and at the upper boundary. The velocity spectrum at the inlet contains energy modes according to the von Kármán energy spectrum [28]. The imposed turbulence intensities trigger bypass transition and turbulence at a downstream location. This is shown in Fig. 1 by the isosurfaces of Q-criterion, which defines a vortex as a continuous fluid region with a positive second invariant of the velocity gradient [29,30], i.e $Q > 0$. The turbulence intensity $Tu = 3\%$ is comparable to the free-stream turbulence intensity used by Brandt et al. [31] who performed numerical simulations that qualitatively reproduced experiments of transition over a flat-plate triggered by grid-generated turbulence.

A grid independence study was performed for the flow case of $M = 6$ (transitional boundary layer) with $Tu = 3\%$ and three grids: $G1 = 661 \times 161 \times 91$, $G2 = 811 \times 201 \times 121$ and $G3 = 1001 \times 251 \times 151$. For the grid spacing calculation the conventional, inner variable, scaling method has been employed, i.e. $\Delta y^+ = u_\tau \Delta y / \nu_w$, where the friction velocity $u_\tau = \sqrt{\tau_w/\rho_w}$, ν_w is the near wall kinematic viscosity; τ_w is the near wall shear stress; and ρ_w is the near wall density. According to the analysis presented in Ref. [25] we consider the present simulations as under-resolved DNS. Properties of the boundary layer are given in Table 1 for the grid $G2$ along with information from a supersonic experiment and comparable (with respect to wall units) previous DNS simulations of fully turbulent hypersonic flows.

Fig. 2 shows the time-averaged van Driest transformed velocity profile and Reynolds normal stresses at the end of the simulation domain for all grids. According to the incompressible "law of the wall" introduced by Theodore von Kármán, the transformed velocity profile should be composed of a linear region close to the wall, followed by a logarithmic overlap region. The present iLES reproduce the linear region and, additionally, the logarithmic region is in excellent agreement with the experimental data of Elena et al. [35] for $M = 2.3$; previous DNS simulations at $M = 6$ [32]; and the logarithmic law proposed by Bradshaw [36], where the constants are derived through experiments. The past experimental and numerical data are from cases corresponding to higher friction Reynolds number, thus higher velocity values in the outer layer are shown. Furthermore, simulations using different grid resolutions predicted the transition region in a similar location within accuracy margin

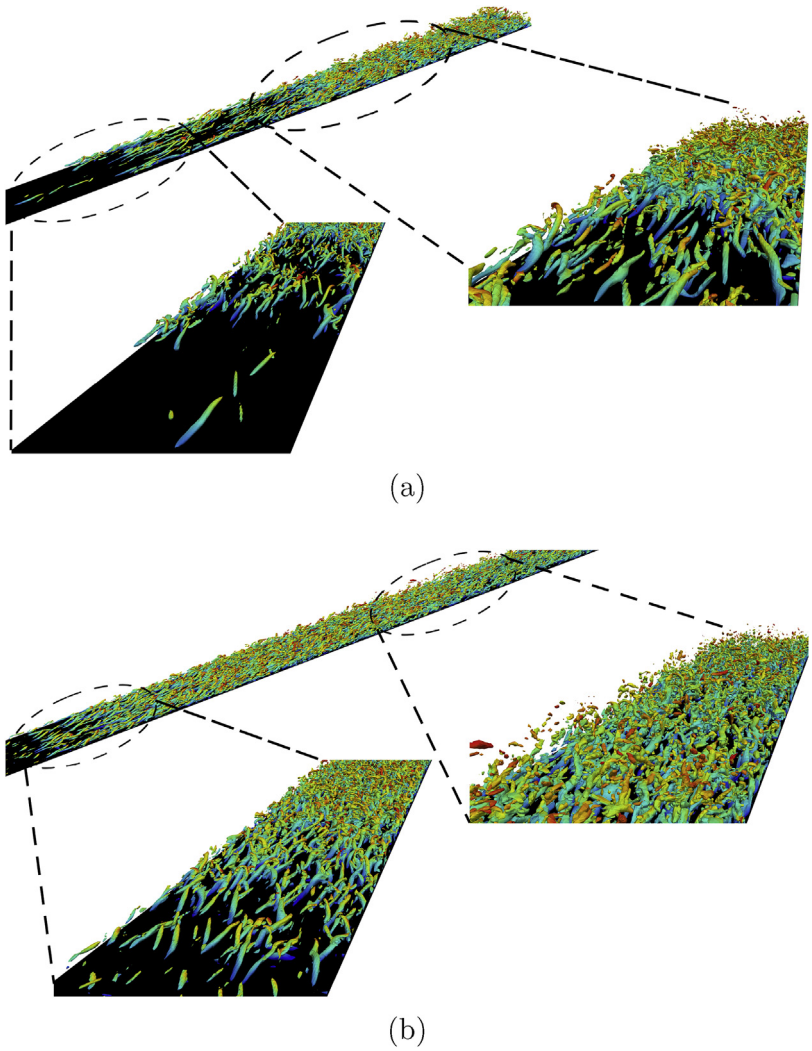

Fig. 1. Isosurfaces of Q-criterion coloured by Mach number highlighting the transitional and fully turbulent regions of the boundary layer for the cases: (a) $M = 6$, $Tu = 0.5\%$, (b) $M = 6$, $Tu = 3\%$ cases, respectively.

of 2%. In view of the above, the analysis and discussion presented below is based on grid *G*2. The spacing in wall units of this grid is $\Delta x^+ = 12.6$, $\Delta y_w^+ = 0.39$, $\Delta y_e^+ = 4.7$ and $\Delta z^+ = 5.5$.

The flow statistics are computed by averaging in time over three flow cycles and spatially in the spanwise direction. The total simulation time for each case is equal to six flow cycles. The calculated amplitudes of the pressure fluctuations and their spectral characteristics are analysed below. The method developed by Welch [37] is used to calculate the power spectral density (PSD) of the pressure fluctuations in specific locations on the wall. The sampling frequency is approximately 500 MHz, with the effective resolution due to grid restrictions being approximately 3.5 MHz. This frequency is high enough to resolve all the spectrum regions that contain the most energetic pressure fluctuations.

3. Acoustic loading

3.1. Spatial analysis

Acoustic loading is expected to peak in the transition region, obtaining significantly higher values than those sustained in the laminar or fully turbulent regions [13,38]. For all cases considered in this paper the pressure fluctuations in the transition region are 38% larger (~3 dB) than their values in the fully turbulent region (Fig. 3a). This results in doubling the amount of energy contained in the pressure fluctuations. Acoustic fatigue experiments on aluminum and composite panel structures have shown that a 3 dB increment is capable to reduce the lifetime of the material by half or more [39,40]. Fig. 3a shows that for higher Mach numbers the peak of pressure fluctuations occurs further downstream, thus indicating a delayed transition.

Table 1
Boundary layer properties at the points of analysis. The lowest Reynolds numbers correspond to the transition region and the highest to the fully turbulent flow. The classification of the simulation type is according to [25] with UR meaning under-resolved.

Ref.	M	Re_τ	Re_θ	Grid points	Sim. Type
Present	4	127–271	3, 456 – 8, 461	20×10^6	UR-DNS
Present	6	88–172	853 – 1, 892	20×10^6	UR-DNS
Present	8	73–119	914 – 1, 665	20×10^6	UR-DNS
[32]	6	–	8, 433	11×10^7	DNS
[14]	5.81	412.8	5, 775.1	22×10^6	DNS
[15]	6	–	2, 652	79×10^6	DNS
[16, 33]	5.85	464	9, 659	64×10^7	UR-DNS
[34]	5.86	453	9, 455	54×10^7	DNS
[35]	2.32	1, 050	4, 700	–	Exp.

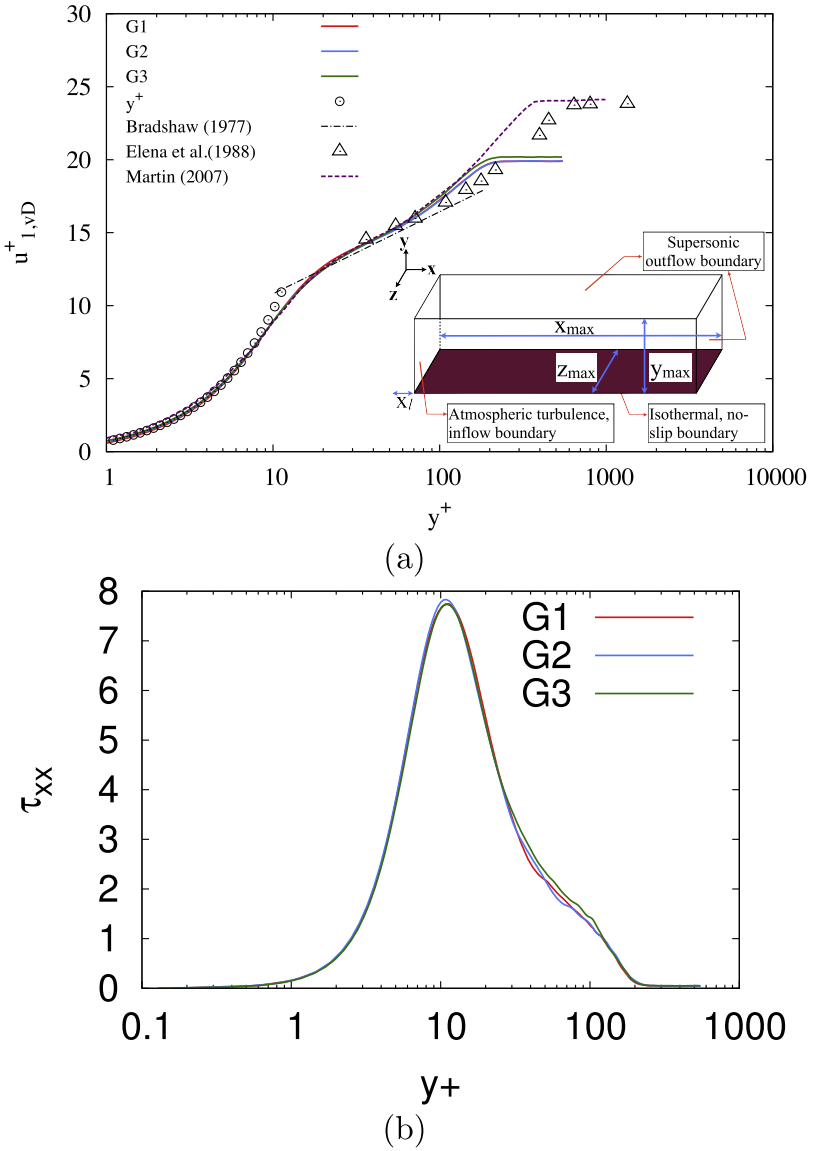

Fig. 2. Results for $M = 6$ and $Tu = 3\%$ for three different grids (G1, G2 and G3). (a) van Driest transformed velocity profile at the end of the simulation domain. The experimental measurements at $M = 2.3$ are from Elena et al. [35]; the Bradshaw's [36] log-law is derived from experimental data; and Martin's DNS [32] corresponds to $M = 6$. The inset is a schematic representation of the simulation domain. (b) Reynolds normal stresses τ_{xx} in outer coordinates at the end of the simulation domain for three different grid resolutions.

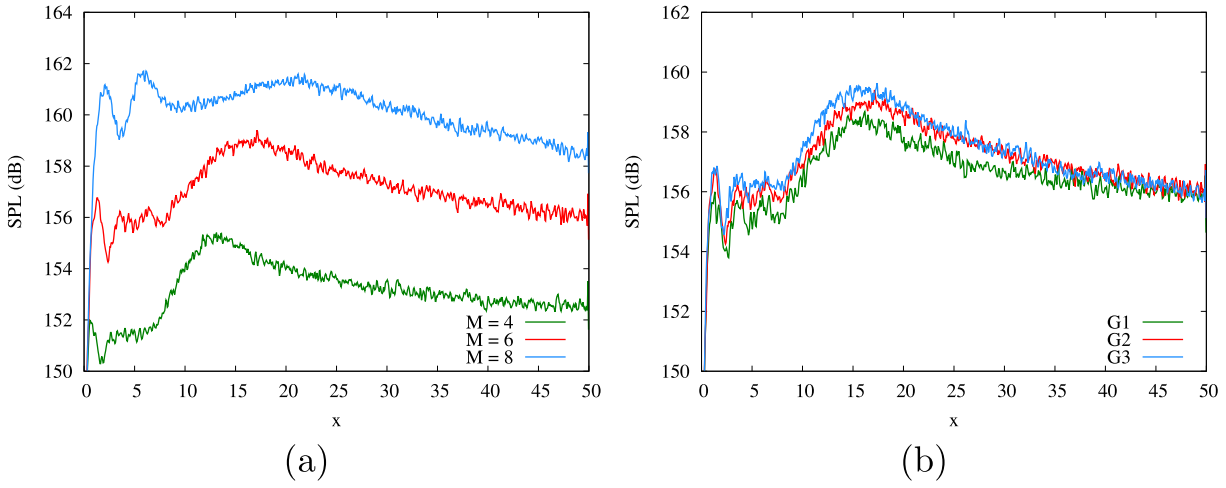

Fig. 3. (a) Mach number effect on SPL calculations at the wall for $Tu = 3\%$. (b) SPL calculations for $M = 6$ and $Tu = 3\%$ for three different grids (G1, G2 and G3); x is the streamwise distance from the inlet non-dimensionalised by x_l.

The difference in acoustic loading between the laminar and transition region is even greater by up to 16 dB for the flows studied here. In Fig. 3b we also demonstrate the excellent grid convergence achieved with respect to SPL calculations along the plate for a representative case.

The (normalised) pressure fluctuations increase when reducing the Mach number (Fig. 4) and this is in agreement with DNS results [33] and experimental measurements [41]. The experimental measurements are presented in three different forms as originally given by Beresh et al. [41]. With black filled-in squares we show the unprocessed/uncorrected data, while with empty squares we show the corrected data with Corcos corrections and noise cancellation. Finally, the star symbols show a further correction of the measured data based on an estimation of the high frequencies that are not captured by the sensors.

Laganelli et al. [3] proposed a theoretical model for P'_{rms}/q_∞ beneath compressible fully turbulent boundary layers, where $q_\infty = (\rho_\infty u_\infty^2)/2$ is the dynamic pressure and u_∞ is the free-stream velocity. The model is based on fitting incompressible measurements [42–45] to compressible flows by taking into account the wall temperature and free-stream Mach number:

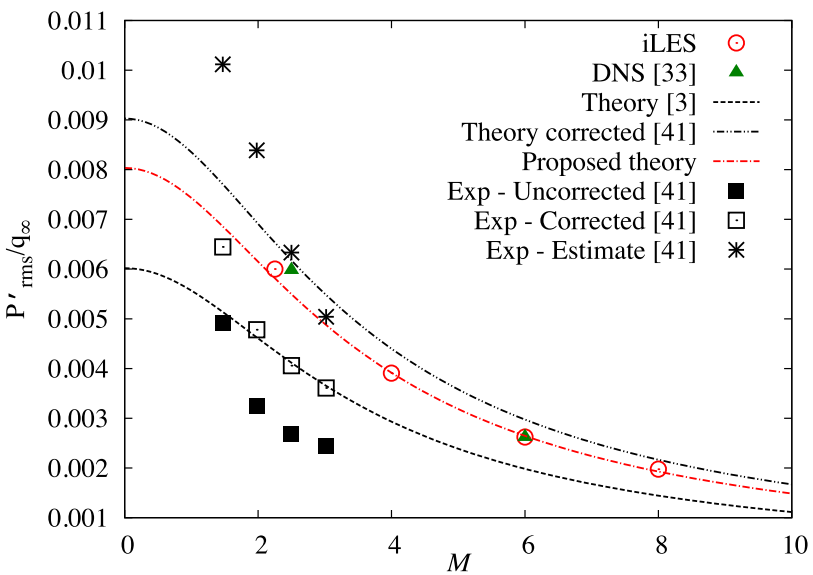

Fig. 4. Root mean square of wall pressure fluctuations (P'_{rms}) in the fully turbulent region normalised by the freestream dynamic pressure, q_∞, versus Mach number. The iLES results are based on the present calculations and Ritos et al. [19] for $M = 2.25$. The lines represent theoretical predictions based on Eq. (1) with $T_w/T_{aw} = 0.99$; see discussion in the text.

$$\frac{P'_{rms}}{q_\infty} = \frac{0.006}{\left[0.5 + (T_w/T_{aw})\left(0.5 + 0.09M_\infty^2\right) + 0.04M_\infty^2\right]^{0.64}}, \tag{1}$$

where T_{aw} is the adiabatic wall temperature calculated from the recovery temperature. The theoretical model (Fig. 4) provides much lower values than the present and past iLES [19], as well as past DNS [33], most likely due to insufficient sensors' spatial resolution [1,46–48].

Previous studies have suggested different values for the numerator of Eq. (1) in the range of 0.008 and 0.010 [1,41,49,50]. Additionally, Gravant et al. [51] suggested that the numerator's value is dependent on Re_θ. Beresh et al. [41] has proposed a value of 0.009 for the incompressible limit based on an estimated extension of the measured pressure spectra (Fig. 4). The present simulations suggest that the value should be 0.008 (Fig. 4). This correction agrees well with DNS [33] and gives better results for a broad range of Mach numbers ($M = 2.25–8$).

The pressure fluctuations in the transition region for three different turbulence intensities are shown in Fig. 5. High levels of turbulence intensity at the inlet ($Tu = 3\%$) result in larger pressure fluctuations in the laminar region, thus ensuring the onset of boundary layer transition. The turbulence intensity influences the location of the maximum acoustic load, but not its value. Downstream of the transition region, the simulations for different turbulent intensities and $M = 6$ converge to the same level of acoustic loading (Fig. 5).

The instantaneous SPLs over the entire wall for the case of $M = 6$ and for three different turbulence intensities shows that vortical structures (VS) are closely associated with higher SPL values (Fig. 6). In the fully turbulent region the average SPL value is about 156 dB. For all turbulence intensities the maximum SPL value of 159 dB is observed in the transition region (Fig. 6). The density gradients also exhibit high values in the same region. Furthermore, at the initial state of the transition, turbulent spots seem to be randomly generated.

Reducing the Mach number, leads to regions of smaller and finely concentrated VS (Fig. 7). The overall acoustic loading on the wall increases with Mach number, e.g. a ~4 dB increase when the Mach number changes from 4 to 6.

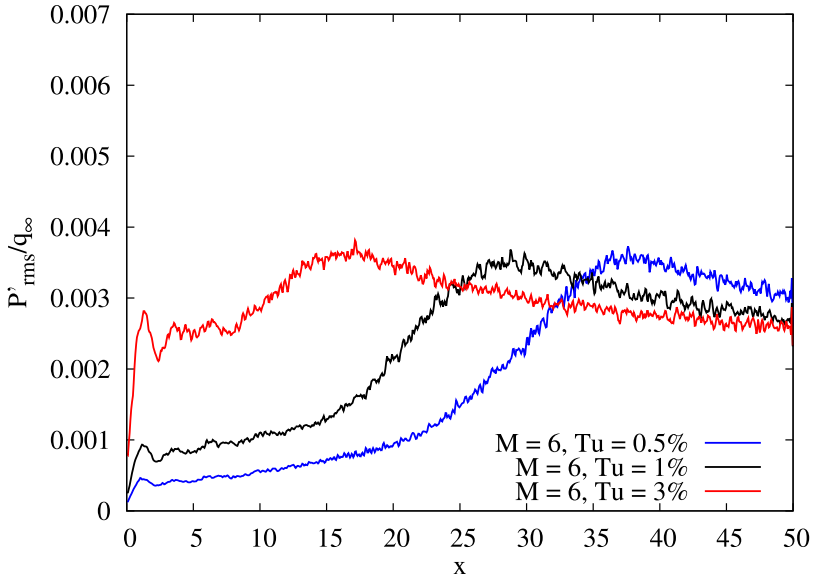

Fig. 5. P'_{rms}/q_∞ along the wall for various turbulent intensities at $M = 6$. x is the streamwise distance from the inlet non-dimensionalised by x_l.

3.2. Spectral analysis

The spectral analysis of the wall pressure fluctuations is based on the single-point spectrum in the frequency domain, which is defined by

$$\Phi(\omega) = \frac{1}{2\pi}\int_{-\infty}^{\infty} \overline{P'(x,y,z,t)P'(x,y,z,t+\tau)}e^{-i\omega\tau}d\tau, \tag{2}$$

where τ is a time delay and ω is the radial frequency. The spectra results are compared with the theoretical predictions for fully turbulent flows [6] and various observations [1]. Bull [1] isolated four different regions of low, mid (which includes the spectral peak), mid-to-high overlap, and high frequencies, with corresponding spectrum slopes of ω^2, ω^0, ω^{-r} ($r = [0.7, 1.1]$),

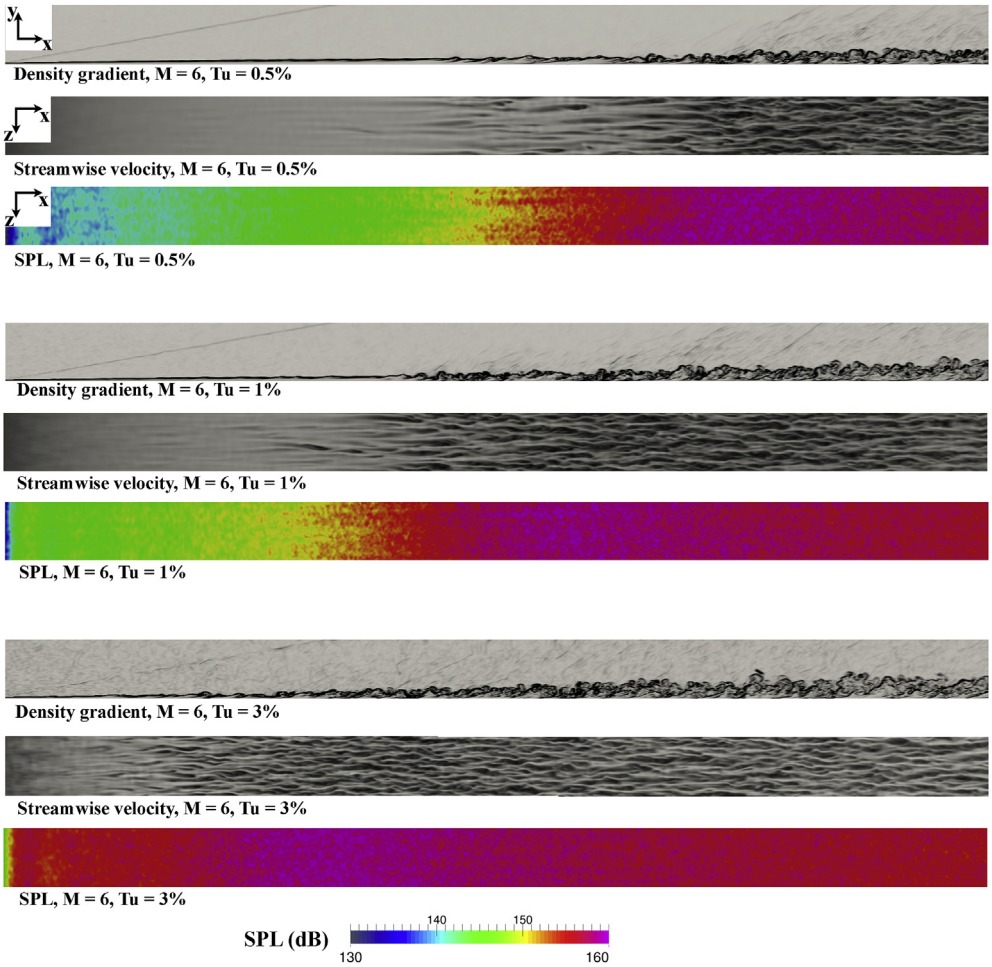

Fig. 6. Instantaneous flow characteristics of the boundary layer at M = 6 and three turbulent intensities at the inflow. The density gradient is a side perspective, while the streamwise velocity and SPL are a top-down perspective. The axes in the $Tu = 0.5\%$ case apply in all other cases too.

and ω^{-t} ($t = [7/3, 5]$), respectively (Fig. 8). The low frequency region is influenced by the turbulent motion in the outer part of the boundary layer, while high frequencies are influenced by the viscosity and turbulent motion in the inner part of the boundary layer.

According to the theoretical arguments made by Ffowcs-Williams [4] for compressible flows, in the low frequency region the scaling should be $\omega \to 0$. This observation has been confirmed by experimental and numerical studies of supersonic and hypersonic turbulent boundary layers [16,34,41,52]. This is in contrast to the Kraichnan-Phillips theorem for incompressible flows [1,53,54], which suggests ω^2.

The mid-to-high overlap frequency region appears at sufficiently high Re_θ values and the spectrum varies as ω^{-r} with $r = 0.7$ to 1.1, influenced by the local Reynolds number. This region is associated with pressure-induced eddies in the logarithmic region of the boundary layer. Its scaling behaviour was predicted by Bradshaw [5], and was verified theoretically [55] and experimentally [41,51].

Following the ω^{-r} region, the spectrum becomes $\omega^{-7/3}$, henceforth called “acoustic-transition”, which was also predicted for isotropic turbulence by Batchelor [56] and has also been observed in various experiments [48,57,58], as well as verified by numerical calculations of supersonic turbulent boundary layers [16,52]. At high frequencies the spectrum decays more rapidly reaching a slope proportional to ω^{-5}. Sources in the sublayer ($y^+ < 20$) contribute to this frequency region according to the theoretical prediction of Blake [6], with the scaling being validated experimentally, as well [51,59].

3.3. Fully turbulent region

The spectra at two positions along the plate are presented. The first location corresponds to the end of the transition region, which is identified as the point of peak pressure fluctuations and depends on the inlet Mach number. The second location ($x = 45$) is located in the fully turbulent flow. These locations were selected in order to discuss the differences of the

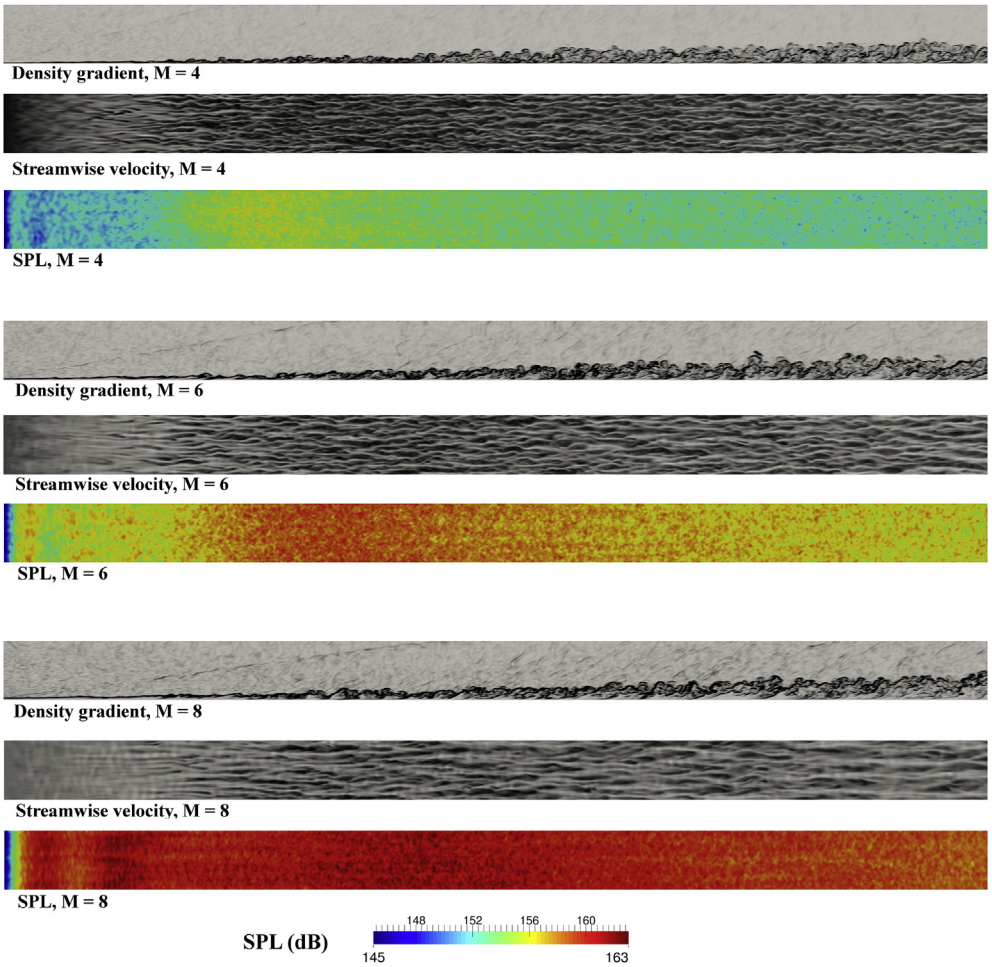

Fig. 7. Instantaneous flow characteristics of the boundary layer for three Mach numbers and Tu = 3%. The density gradient is a side perspective, while the streamwise velocity and SPL are a top-down perspective. The axes in 6 ($Tu = 0.5\%$ case) apply in all cases here.

transitional and fully turbulent regions. The spectrum roll-off of the fully turbulent flow is shown in Fig. 9. All spectra have been filtered with the 'smooth bezier' function of Gnuplot in order to highlight the various scaling regions more clearly. Fig. 9b shows both the raw and the filtered PSD. The spectrum roll-off is not affected by filtering. Fig. 9d shows a characteristic non-filtered spectrum where grid convergence is achieved. The low frequency pressure fluctuations are nearly grid-converged. The magnitude of the high-frequency spectrum is under-predicted on the coarsest grid (G1).

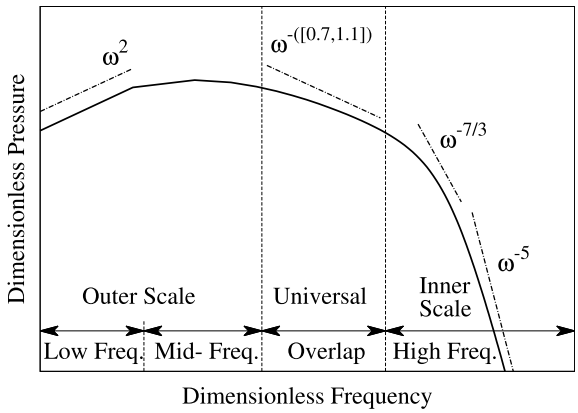

Fig. 8. Frequency regions isolated through collective observations by Bull [1].

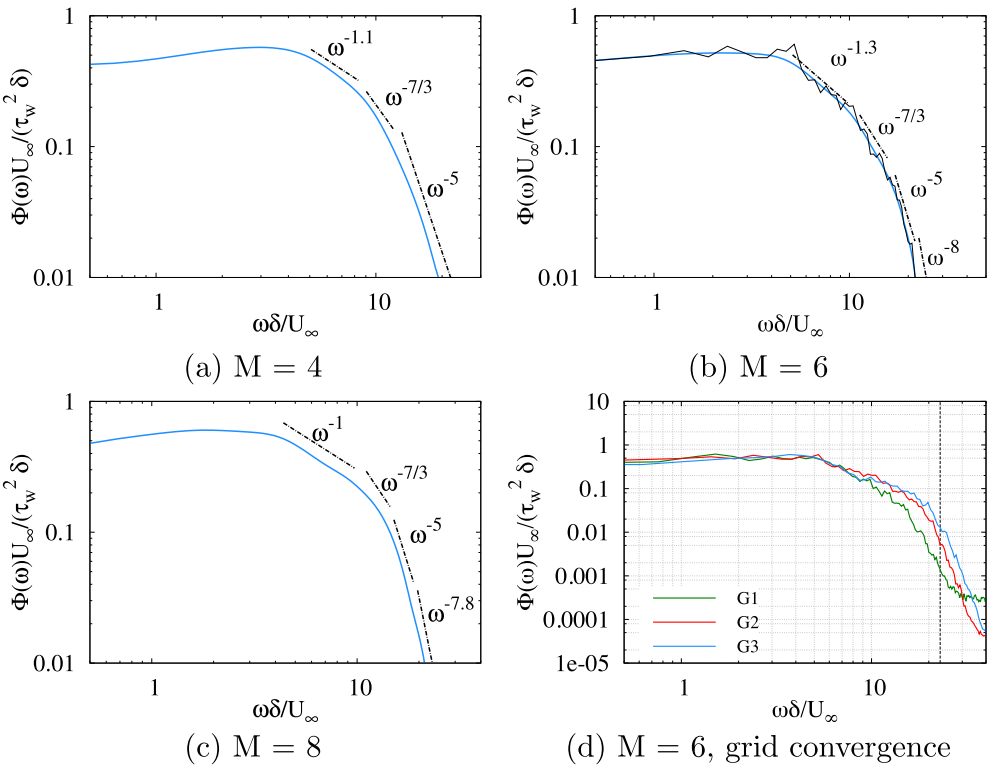

Fig. 9. PSD in the fully turbulent region. The dashed vertical line in (d) indicated the maximum frequency resolved by mesh G2.

The low frequency region yields $\omega \to 0$, which agrees with the aforementioned analysis. The mid-to-high overlap frequency region scales as ω^{-r} with the frequency range and slope being Mach number dependent. The value of r lies between 1.0 and 1.3 depending on the Mach number. This region also occurs over a broader range of frequencies, as the Mach number increases.

The high frequency region of the spectrum, including the "acoustic-transition" scaling (Fig. 8), also appears in the case of hypersonic turbulent boundary layers. Additionally, the last leg of the high frequency encompasses a region of (approximately) ω^{-8} at $M = 6$ and 8. We attribute this region to high-speed, compressibility effects closer to the wall ($y^+ < 20$). The Mach dependence of the spectrum in fully turbulent boundary layers has also been observed in experiments [60] and numerical simulations [16]. Due to the quasi-incompressible nature of the flow near the (iso-thermal) wall, the temperature fluctuations are significantly reduced.

3.4. End of the transition region

The largest pressure fluctuations occur in the transition region (Figs. 3a and 5) and the spectra results are shown in Fig. 10. Note that for all Mach numbers the transition region contains considerably more low-frequency pressure fluctuations compared to the fully turbulent boundary layer.

In the low frequency region, the simulations yield $\omega^{0.3}$ for all Mach numbers. The rest of the spectrum depends strongly on the Mach number. For $M = 4$ the mid-frequency region is a plateau, while for $M = 6$ and $M = 8$ the scaling yields $\omega^{-0.5}$ and $\omega^{-0.8}$, respectively. In the "acoustic-transition" region the scaling yields ω^{-3}, $\omega^{-1.6}$ and $\omega^{-2.8}$ for $M = 4$, $M = 6$ and $M = 8$, respectively. It is clear that the scaling of the spectra at the end of the transition region is different than Batchelor's theoretical prediction of $\omega^{-7/3}$, which was based on the assumption of isotropic turbulence. The deviation of the scaling behaviour from $\omega^{-7/3}$ due to the onset of flow anisotropy and localised coherent structures. Near the wall, turbulent flow structures are highly anisotropic having an ellipsoidal shape [27]. The streamwise turbulent structures are dominant in the mid-buffer layer region; for a supersonic flow ($M = 2.5$) this is around $y^+ \approx 10$ [27].

In the high frequency regime the spectrum scales with ω^{-5}, $\omega^{-6.8}$ and $\omega^{-7.8}$ for the three Mach numbers (Fig. 10). Therefore, the high frequency flow regime at the end of the transition region approaches the spectral behaviour of the fully turbulent flow for all Mach numbers. The spectrum's decay is accelerated when increasing the Mach number, namely ω^{-5} for $M = 4$ and ω^{-8} for $M = 6$ and $M = 8$, respectively.

The new spectra scaling applicable to the end of the transition region is summarised in Fig. 11. The low frequency regime scales with $k = 0.3$, while the rest of the spectrum is Mach number dependent. The scaling lies in the intervals $r = [0.5, 0.8]$,

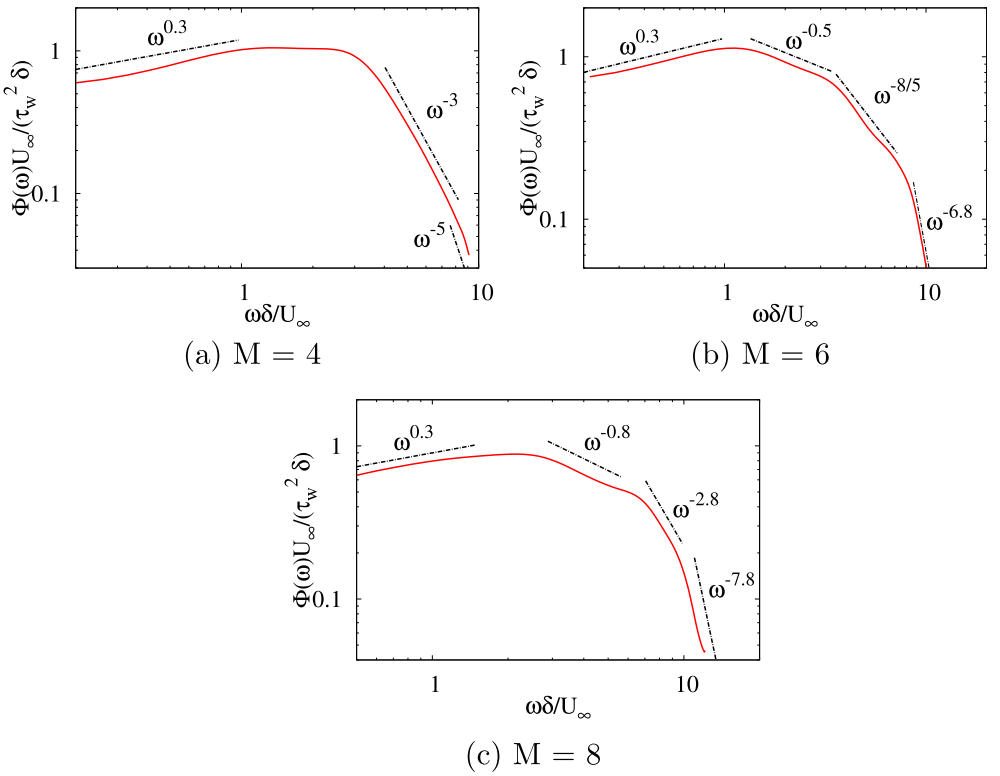

Fig. 10. PSD at the end of the transition region.

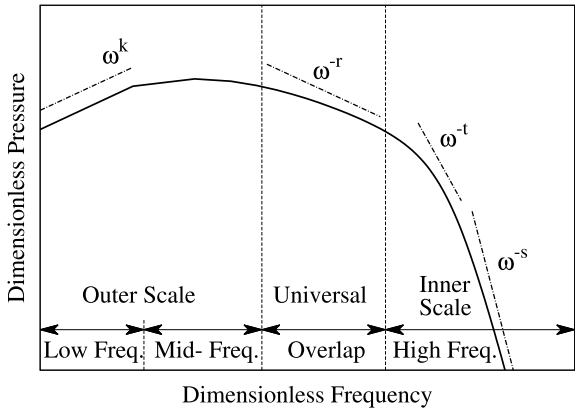

Fig. 11. Frequency regions in the transition flow region. The scaling factors are: $k = 0.3$, $r = [0.5, 0.8]$, $t = [1.6, 3.0]$ and $s = [5, 7.8]$. The r scaling does not appear at $M = 4$.

$t = [1.6, 3.0]$ and $s = [5, 7.8]$ for the mid-to-high frequency overlap, "acoustic-transition" from overlap to high frequency, and high-frequency region, respectively.

3.5. Turbulent intensity effects

The turbulent intensity has a small effect on the spectrum at the end of the transition region (Fig. 12a). For $Tu = 0.5\%$ and $Tu = 1.0\%$ the Reynolds number is slightly higher than $Tu = 3.0\%$, thus the spectra for the first two cases are in closer agreement. For $Tu = 0.5\%$, the mid-frequency region of $\omega^{-0.5}$ appears only within a short range of frequencies.

In the fully turbulent flow, the friction Reynolds number is similar for all turbulent intensities. The turbulent intensity influences only the overlap region and the initial part of the high frequency region. The pre-multiplied pressure spectra

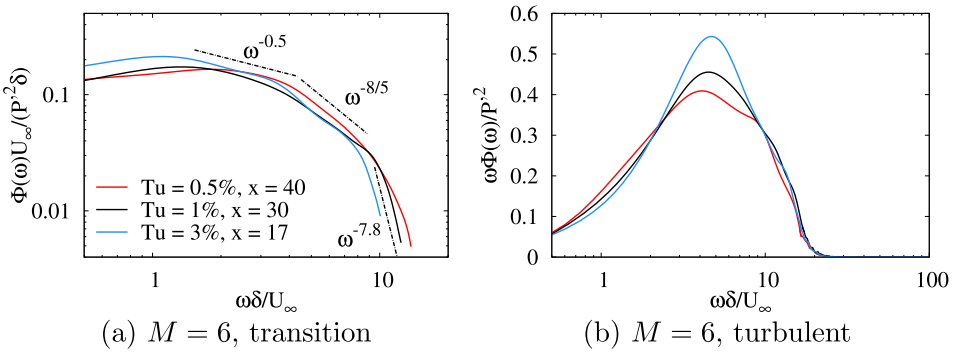

Fig. 12. Turbulent intensity effects on the PSD of pressure fluctuations: (a) at the end of transition region where the peak of P'_{rms} magnitude is calculated; (b) fully turbulent locations with the same Re_τ. Turbulent intensity effects on the pre-multiplied PSD of the pressure fluctuations. The different x locations correspond to the end of the transition region.

(Fig. 12b) show that the maximum value occurs in the same position irrespective of the turbulent intensity value. However, a higher turbulent intensity results in a higher amplitude due to the higher energy content of the fluctuation imposed at the inlet.

4. Conclusions

Acoustic effects beneath hypersonic transitional boundary layers have been investigated by performing spatial and spectral analysis of near-wall pressure fluctuations. iLES at different Mach numbers and a range of inlet turbulent intensities have been carried out. The simulations have also been validated against DNS and experimental data. The most important conclusions drawn from the present study are summarised below:

- Laganelli's theoretical model, applicable to the incompressible limit, was modified and validated against iLES, DNS and experimental data for a range of Mach numbers.
- Increasing the turbulence intensity of the free-stream turbulence influences the location of the maximum acoustic load but not its magnitude.
- High SPL values are associated with vortical structures of large streamwise velocity.
- Structural panels will be subjected to the strongest acoustic fatigue in the transition region.
- Spectral analysis was performed at two points, at the end of the transition and in the fully turbulent flow, and revealed the following:
  (i) The frequency spectrum is Mach number dependent both for transitional and fully turbulent flows.
  (ii) The pressure fluctuations in transitional flows are governed by scaling laws that differ from the ones in turbulent flows. New scaling laws for the wall-pressure fluctuations in the transition region have been presented.
  (iii) Increasing the free-stream turbulence intensity leads to larger fluctuations in the fully turbulent region.

Future research should aim at the development of improved acoustic models for transitional and fully turbulent compressible flows, as well as investigation of the effects of acoustic loading on the structural vibration and fatigue of aerospace structures.

Acknowledgements

This work was sponsored by the Air Force Office of Scientific Research, Air Force Material Command, USAF, under grant number FA9550-14-1-0224. The U.S. Government is authorised to reproduce and distribute reprints for Governmental purpose notwithstanding any copyright notation thereon. The authors would like to thank S. M. Spottswood and Z. Riley at AFRL Structural Sciences Center, as well as D. Garner (EOARD) for their support. Results were obtained using the EPSRC funded ARCHIE-WeSt High Performance Computer (www.archie-west.ac.uk) under EPSRC grant no. EP/K000586/1.

References

[1] M.K. Bull, Wall-pressure fluctuations beneath turbulent boundary layers: some reflections on forty years of research, J. Sound Vib. 190 (3) (1996) 299–315.
[2] S.R. Pate, M.D. Brown, Acoustic Measurements in Supersonic Transitional Boundary Layers, Tech. Rep. AEDC-TR-69-182, ARO Inc, 1969.
[3] A.L. Laganelli, A. Martellucci, L.L. Shaw, Wall pressure fluctuations in attached boundary-layer flow, AIAA J. 21 (4) (1983) 495–502.
[4] J.E. Ffowcs-Williams, Surface pressure fluctuations induced by boundary layer flow at finite Mach number, J. Fluid Mech. 22 (1965) 507–519.

[5] P. Bradshaw, Inactive motion and pressure fluctuations in turbulent boundary layers, J. Fluid Mech. 30 (2) (1967) 241–258.
[6] W.K. Blake, Mechanics of Flow-induced Sound and Vibration, Academic Press, New York, 1986.
[7] J.C. Houbolt, On the Estimation of Pressure Fluctuations in Boundary Layers and Wakes, Tech. Rep. TIS 66SD296, General Electric, 1966.
[8] L.M. Mack, Boundary Layer Linear Stability Theory, Tech. Rep. 709, AGARD, 1984.
[9] J. Sivasubramanian, H.F. Fasel, Direct numerical simulation of transition in a sharp cone boundary layer at mach 6: fundamental breakdown, J. Fluid Mech. 768 (2015) 175–218.
[10] C.-H. Zhang, Q. Tang, C.-B. Lee, Hypersonic boundary-layer transition on a flared cone, Acta Mech. Sin. 29 (1) (2013) 48–53.
[11] K.M. Casper, S.J. Beresh, S.P. Schneider, Pressure fluctuations beneath instability wavepackets and turbulent spots in a hypersonic boundary layer, J. Fluid Mech. 756 (2014) 1058–1091.
[12] Y. Zhu, C. Zhang, X. Chen, H. Yuan, J. Wu, S. Chen, C. Lee, Transition in hypersonic boundary layers: role of dilatational waves, AIAA J. 54 (10) (2016) 3039–3049.
[13] K.M. Casper, S.J. Beresh, J.F. Henfling, R.W. Spillers, B.O.M. Pruett, Hypersonic wind-tunnel measurements of boundary-layer transition on a slender cone, AIAA J. 54 (4) (2016) 1250–1263.
[14] L. Duan, I. Beekman, M.P. Martín, Direct numerical simulation of hypersonic turbulent boundary layers. Part 3. Effect of Mach number, J. Fluid Mech. 672 (2011) 245–267.
[15] K.J. Franko, S.K. Lele, Breakdown mechanisms and heat transfer overshoot in hypersonic zero pressure gradient boundary layers, J. Fluid Mech. 730 (2013) 491–532.
[16] L. Duan, M.M. Choudhari, C. Zhang, Pressure fluctuations induced by a hypersonic turbulent boundary layer, J. Fluid Mech. 804 (2016) 578–607.
[17] D. Drikakis, Advances in turbulent flow computations using high-resolution methods, Prog. Aero. Sci. 39 (6–7) (2003) 405–424.
[18] D. Drikakis, M. Hahn, A. Mosedale, B. Thornber, Large eddy simulation using high resolution and high order methods, Proc. R. Soc. A 367 (2009) 2985–2997.
[19] K. Ritos, I.W. Kokkinakis, D. Drikakis, S.M. Spottswood, Implicit large eddy simulation of acoustic loading in supersonic turbulent boundary layers, Phys. Fluids 29 (4) (2017) 1–11.
[20] E.F. Toro, Riemann Solvers and Numerical Methods for Fluid Dynamics, third ed., Springer, 2009.
[21] D.S. Balsara, C.W. Shu, Monotonicity preserving weighted essentially non-oscillatory schemes with increasingly high order of accuracy, J. Comput. Phys. 160 (2) (2000) 405–452.
[22] D. Drikakis, W. Rider, High-resolution Methods for Incompressible and Low-speed Flows, Springer, 2005.
[23] F. Grinstein, L. Margolin, W. Rider (Eds.), Implicit Large Eddy Simulation: Computing Turbulent Fluid Dynamics, Cambridge University Press, 2007.
[24] I.W. Kokkinakis, D. Drikakis, Implicit large eddy simulation of weakly-compressible turbulent channel flow, Comput. Methods Appl. Math. 287 (2015) 229–261.
[25] K. Ritos, I.W. Kokkinakis, D. Drikakis, Performance of high-order implicit large eddy simulations, Comput. Fluids 178 (2018) 307–312, https://doi.org/10.1016/j.compfluid.2018.01.030.
[26] K. Ritos, I.W. Kokkinakis, D. Drikakis, Physical insight into a mach 7.2 compression corner flow, in: AIAA Aerospace Sciences Meeting, Kissimmee, Florida, 2018.
[27] K. Ritos, I.W. Kokkinakis, D. Drikakis, Physical insight into the accuracy of finely-resolved iLES in turbulent boundary layers, Comput. Fluids 169 (2018) 309–316.
[28] D.K. Wilson, Turbulence Models and the Synthesis of Random Fields for Acoustic Wave Propagation Calculations, Tech. Rep. ARL-TR-1677, Army Research Laboratory, 1998.
[29] J.C.R. Hunt, A.A. Wray, P. Moin, Eddies, Streams, and Convergence Zones in Turbulent Flows, Tech. rep., Center for Turbulence Research, 1988.
[30] V. Kolář, J. Šístek, Corotational and compressibility aspects leading to a modification of the vortex-identification q-criterion, AIAA J. 53 (8) (2015) 2406–2410.
[31] L. Brandt, P. Schlatter, D.S. Henningson, Transition in boundary layers subject to free-stream turbulence, J. Fluid Mech. 517 (2004) 167–198.
[32] M.P. Martín, Direct numerical simulation of hypersonic turbulent boundary layers. Part 1. initialization and comparison with experiments, J. Fluid Mech. 570 (2007) 347–364.
[33] L. Duan, M.M. Choudhari, Numerical study of pressure fluctuations due to a Mach 6 turbulent boundary layer, in: 51st AIAA Aerospace Sciences Meeting, 2013, pp. 1–16.
[34] C. Zhang, L. Duan, M.M. Choudhari, Effect of wall cooling on boundary-layer-induced pressure fluctuations at Mach 6, J. Fluid Mech. 822 (2017) 5–30.
[35] M. Eléna, J.P. Lacharme, Experimental study of a supersonic turbulent boundary layer using a laser Doppler anemometer, J. Mec. Theor. Appl. 7 (2) (1988) 90–175.
[36] P. Bradshaw, Compressible turbulent shear layers, Annu. Rev. Fluid Mech. 9 (1977) 33–54.
[37] P.D. Welch, The use of Fast Fourier Transform for the estimation of power spectra: a method based on time averaging over short, modified periodograms, IEEE Trans. Audio Electroacoust. AU-15 (1967) 70–73.
[38] A. Martellucci, L. Chaump, D. Rogers, D. Smith, Experimental determination of the aeroacoustic environment about a slender cone, AIAA J. 11 (5) (1973) 635–642.
[39] B.J. Moskal, Investigation of the Sonic Fatigue Characteristics of Randomly Excited Aluminum, Tech. Rep. CR-425, NASA, 1966.
[40] J. Soovere, The effect of acoustic/thermal environments on advanced composite fuselage panels, J. Aircraft 22 (4) (1985) 257–263.
[41] S.J. Beresh, J.F. Henfling, R.W. Spillers, B.O.M. Pruett, Fluctuating wall pressures measured beneath a supersonic turbulent boundary layer, Phys. Fluids 23 (075110) (2011) 1–16.
[42] R.D. Shattuck, Sound Pressures and Correlations of Noise on the Fuselage of a Jet Aircraft in Flight, Tech. Rep. TN-D-1086, NASA, 1961.
[43] W.W. Willmarth, C.E. Wooldridge, Measurements of the fluctuating pressure at the wall beneath a thick turbulent boundary layer, J. Fluid Mech. 14 (2) (1962) 187–210.
[44] W.W. Willmarth, F.W. Roos, Resolution and structure of the wall pressure field beneath a turbulent boundary layer, J. Fluid Mech. 22 (1) (1965) 81–94.
[45] M.K. Bull, Wall-pressure fluctuations associated with subsonic turbulent boundary layer flow, J. Fluid Mech. 28 (4) (1967) 719–754.
[46] W.W. Willmarth, Pressure fluctuations beneath turbulent boundary layers, Annu. Rev. Fluid Mech. 7 (1975) 13–36.
[47] M.K. Bull, A.S.W. Thomas, High frequency wall-pressure fluctuations in turbulent boundary layers, Phys. Fluids 19 (4) (1976) 597–599.
[48] G. Schewe, On the structure and resolution of wall-pressure fluctuations associated with turbulent boundary layer flow, J. Fluid Mech. 134 (1983) 311–328.
[49] R.M. Lueptow, Transducer resolution and the turbulent wall pressure spectrum, J. Acoust. Soc. Am. 97 (1) (1995) 370–378.
[50] M.C. Goody, R.L. Simpson, Surface pressure fluctuations beneath two= and three-dimensional turbulent boundary layers, AIAA J. 38 (10) (2000) 1822–1831.
[51] S.P. Gravante, A.M. Naguip, C.E. Wark, H.M. Nagib, Characterization of the pressure fluctuations under a fully developed turbulent boundary layer, AIAA J. 36 (10) (1998) 1808–1816.
[52] M. Bernardini, S. Pirozzoli, Wall pressure fluctuations beneath supersonic turbulent boundary layers, Phys. Fluids 23 (085102) (2011) 1–11.
[53] R.H. Kraichnan, Pressure fluctuations in turbulent flow over a flat plate, J. Acoust. Soc. Am. 28 (3) (1956) 378–390.
[54] O.M. Phillips, On the aerodynamic surface sound from a plane turbulent boundary, Proc. R. Soc. A 234 (1198) (1956) 327–335.
[55] R.L. Panton, J.H. Linebarger, Wall pressure spectra calculations for equilibrium boundary layers, J. Fluid Mech. 65 (2) (1974) 261–287.
[56] G.K. Batchelor, Pressure fluctuations in isotropic turbulence, Proc. Camb. Phil. Soc. 47 (1951) 359–374.
[57] Y. Tsuji, T. Ishihara, Similarity scaling of pressure fluctuation in turbulence, Phys. Rev. E 68 (2003), 026309.

[58] R. Camussi, M. felli, F. Pereira, G. Aloisio, A.D. Marco, Statistical properties of wall pressure fluctuations over a forward-facing step, Phys. Fluids 20 (2008), 075113.
[59] T.M. Farabee, M.J. Casarella, Spectral features of wall pressure fluctuations beneath turbulent boundary layers, Phys. Fluids A 3 (10) (1991) 2410–2420.
[60] J. Laufer, Some statistical properties of the pressure field radiated by a turbulent boundary layer, Phys. Fluids 7 (8) (1964) 1191–1197.